The Thesis Committee for Qianru Jia
Certifies that this is the approved version of the following thesis:

Synthesis and Characterization of High-Surface Area Hexagonal Boron Nitride Foam Structures

APPROVED BY
SUPERVISING COMMITTEE:

Li Shi, Supervisor

Yaguo Wang

Synthesis and Characterization of High-Surface Area Hexagonal Boron Nitride Foam Structures

by

Qianru Jia

Thesis

Presented to the Faculty of the Graduate School of

The University of Texas at Austin

in Partial Fulfillment

of the Requirements

for the Degree of

Master of Science in Engineering

The University of Texas at Austin

May 2019

Acknowledgements

I would like to thank my parents for their constant love and support, as well as for their inspirations and encouragement for my academic goals and graduate study. I would also like to thank all my friends for helping relieve my pressure and entertainment. I would like to deliver my thanks to Dr. Evan Fleming and Dr. David Choi for mentoring me at the beginning of my work, Dr. Sean Evan Sullivan and Dr. Xi Chen for their great suggestion and guidance on experimental equipment, and all my group members for their helpful and valuable discussions on my project. In particular, I really appreciate having Professor Li Shi as my supervisor. His continuous patience, enthusiasm, and encouragement motivates me to pursue my objective faithfully. It is incredibly fortunate to work with an erudite professor who has a sincere passion for his concentrations. Last but not the least, I would like to thank every day and night I spent in the laboratory and behind the screen, every failure and setback I faced in my life, and every applause and happiness I experienced after the fight. These all write down my growth and progress and will continue to make me stronger in the future.

Abstract

Synthesis and Characterization of High-Surface Area Hexagonal Boron Nitride Foam Structures

Qianru Jia, M.S.E

The University of Texas at Austin, 2019

Supervisor: Li Shi

Hexagonal boron nitride (h-BN) shares a similar layered crystal structure as graphite. Graphite is a semimetal with an ultrahigh thermal conductivity. In comparison, h-BN is a high-thermal conductivity electrical insulator, which is more suitable than metals for a number of applications in thermal management of electronic devices. Continuous and porous foam structures of both graphitic carbon and h-BN have been synthesized for thermal management and other applications. High-thermal conductivity and light-weight graphite foams have demonstrated superior thermal performance than both metal foams and van der Waals bonded networks of carbon nanotubes and graphitic flakes. However, the volume fraction and effective thermal conductivity of existing h-BN foam structures are still limited by the large pore size and limited specific surface area of the sacrificial reticular nickel foam templates used for chemical vapor deposition (CVD) of h-BN. This thesis reports on an investigation of the use of sacrificial sintered nickel powder templates with reduced pore sizes to increase the surface area of h-BN foam grown by atmospheric pressure CVD (APCVD) on the template. The volume fraction of the obtained h-BN foam

is increased by a factor of 2.8 compared to a baseline h-BN foam grown on a commercial reticular nickel foam template. With poly(methyl methacrylate) (PMMA) filled into the pore space of the h-BN foam, the room-temperature effective thermal conductivity of the composite increases from 0.31 ± 0.02 $Wm^{-1}K^{-1}$ for the baseline structure to 0.51 ± 0.04 $Wm^{-1}K^{-1}$ for the structure with increased h-BN volume fraction. The room-temperature solid thermal conductivity of the h-BN strut is determined from the effective thermal conductivity via the Lemlich model to be 380 ± 80 $Wm^{-1}K^{-1}$, which is comparable to literature basal-plane values for h-BN crystals and compressed pellets. For a h-BN foam structure annealed at 700°C upon growth for 48 hrs, the solid thermal conductivity is 490 ± 120$Wm^{-1}K^{-1}$.

Table of Contents

List of Tables

List of Figures

Chapter 1 Introduction

In the semiconductor industry, Moore's Law has been followed closely until recently. This law projects that the number of transistors on a computer chip will double every two years.[1] The increased transistor density is accompanied with increased heat dissipation density, which has reached over 100 W cm^{-2}.[2] Due to the difficulties in preventing the computer chip from overheating under the large heat density,[3] thermal management has become the key challenge for the semiconductor industry to follow Moore's law. This challenge opens up opportunities for innovations in thermal management materials, devices, and systems for microelectronics.[4] Similar challenges and opportunities exist in energy technologies such as thermal energy storage systems for both high-temperature concentrated solar thermal power and near room-temperature cooling and heating of buildings and vehicles.

The open cellular foam of a high-thermal conductivity material is one type of materials structures that have been investigated for thermal management applications. The continuous interconnected strut network serves as effective pathways for heat conduction from the functional materials, such as a phase change material (PCM) for thermal energy storage, which are filled into the pore space of the foam structure.[5] Compared to van der Waals bonded networks of high-thermal conductivity nanomaterials such as metal nanowires, carbon nanotubes, and graphitic flakes, the internal interface thermal resistance is greatly reduced in a continuous foam structure.[6]

Among the different foam structures, graphitic carbon foams exhibit several desirable properties including low atomic mass, high solid thermal conductivity, and mechanical flexibility. Different methods have been reported for the synthesis of a variety of carbon foams from amorphous carbon,[7] graphite,[8] expanded graphite,[9,10] and graphene

oxide.[11] High-density graphitic foams have been synthesized with mesophase pitches as a precursor based on calcination and carbonization processes involving temperatures as high as about 2500°C and pressure on the MPa level.[12] The template carbonization method is based on impregnating polyurethane foam with poly(amic acid), followed by imidization and carbonization at a high temperature up to 3000°C.[7] Besides these high-temperature processes, carbon foams have also been synthesized with the use of the Pechini method, also called sol-gel route, which involves an intensive mixture of positive ions in a solution, formation of a polymer gel and deformation of the obtained metal-polymer composition to a highly homogenous oxide precursor.[7] Meanwhile, exfoliated graphite has been compressed into graphitic foam structures.[12] Compared to these methods, chemical vapor decomposition (CVD) of graphite foams on a sacrificial nickel foam catalytic template has emerged as an effective approach for the growth of low-density, high-crystalline quality graphite foams.[13,14]

The thermal performance of the carbon foams depends on the crystalline quality, strut wall thickness, and the pore size. The mean pore size of activated carbon foam influences the thermal properties. Large pores limit the specific surface area and result in a large distance and resistance from the filled functional materials to the high-thermal conductivity matrix. Efforts have been made to grow long carbon nanotubes on the strut wall of CVD ultrathin graphite foam to increase the specific surface area and reduce the resistance of heat transport from the PCM inside the pore space to the graphite strut walls.[15,16] The obtained effective thermal conductivity was increased by a factor of 1.8 compared to that of a graphite-PCM composite. Recently, nickel powers have been sintered to form catalytic templates for CVD growth of graphite foam structures.[17] The low-cost nickel powder can reduce the pore size and increase the specific surface area up to 68 times compared to the reticulated nickel template. Because of the large increase in the volumetric

specific surface area, the graphite volume fraction and the effective thermal conductivity have been increased from 0.87 ± 0.09% and 2.1 ± 0.3 $Wm^{-1}K^{-1}$ to 8.4 ± 0.3% and 16.3 ± 1.1 $Wm^{-1}K^{-1}$, respectively.

Despite the progress in the growth of high-thermal conductivity graphite foam, the semi-metallic nature of graphite limits its use for some thermal management applications. For example, thermally conducting and electrically insulating filler materials are needed for increasing the thermal performance of polymeric materials used to join adjacent chips in three-dimensional (3D) integrated circuit (IC) architecture.[3] This requirement can potentially be made with the use of hexagonal boron nitride (h-BN) to replace graphitic materials as the high-thermal conductivity fillers. Both graphite and h-BN are two-dimensional (2D) layered materials. The basal-plane and inter-layer lattice constants are a_0 = 2.504 Å and c_0=6.661 Å for h-BN. These values are similar to those of graphite, a_0 = 2.456Å and c_0=6.696 Å.[18] However, the large band gap of 5.97 eV makes h-BN essentially an electrical insulator.[24] Due to its mechanical robustness and flexibility, chemical stability, and high basal-plane thermal conductivity, h-BN has been investigated for thermal management applications.[18-21] As an electrical insulator and thermal conductor, h-BN has been employed for both electric insulation and heat dissipation in applications ranging from electronic packaging, electrical shielding, flexible substrates, and advanced heterostructure devices.[22-25]

Recently, h-BN has been grown with CVD including atmospheric pressure chemical vapor deposition (APCVD).[26-29] In one CVD synthesis on reticulated Ni catalytic templates,[25] 3D-C and 3D h-BN are hybridized into a 3D-BNC network. The highly porous structure allows the graphite-h-BN hybrid foam to achieve low density and light weight while maintaining its structural integrity and flexural toughness. In another h-BN growth using the ammonia-borane ($H_3N–BH_3$) precursor at different Ar/H_2 background

pressures,[30] both the growth rate and the disorder increase with the growth pressure. In addition, solid borazane precursor and Ni foam templates have been used in low-pressure CVD (LPCVD) growth of free-standing h-BN foams with an ultralow density of 1.6 mg/cm^3.[31] Meanwhile, an APCVD method has been used to grow h-BN foams on Ni foam templates.[32,33] At a h-BN volume fraction of 0.076 ± 0.01%, the effective thermal conductivity of h-BN-Poly(methyl methacrylate) (PMMA) composite increased from 0.34 ± 0.03 $Wm^{-1}K^{-1}$ at room temperature to 0.73 ± 0.07 $Wm^{-1}K^{-1}$ at 140 K. The temperature dependence is due to the lattice thermal conductivity of crystalline h-BN, and is opposite to that of amorphous PMMA.

The effective thermal conductivity of existing h-BN foams are limited by the low h-BN volume fraction, which is limited by both the surface area provided by the Ni foam template and the small h-BN thickness that can be grown using the solid precursor. In this thesis, small particle size nickel powders are sintered at about ~1100°C to form Ni -powder templates to obtain a relatively high specific surface area compared to commercial reticulated Ni foam. The sacrificial sintered Ni powder template is used to grow h-BN foams structures. PMMA-h-BN composites are prepared for thermal transport measurements to determine the effect of increased surface area of the Ni template on the effective thermal conductivity and basal-plane thermal conductivity of h-BN.

Chapter 2 Synthesis and Characterization of High-Surface Area Hexagonal Boron Nitride

This chapter describes APCVD synthesis of h-BN foams on both commercial nickel foam and sintered Ni powder foam templates. The obtained h-BN foams are impregnated by Poly(methyl methacrylate) (PMMA) to form h-BN-PMMA composites and are characterized via Laser Flash Analysis (LFA) and Differential Scanning Calorimetry (DSC). The thermal properties results are compared in the following sections.

2.1 Synthesis of High-Surface Area Hexagonal Boron Nitride Foam

Commercial Ni foam is a common template used for APCVD growth of graphite and h-BN foam structures. However, the pore size is as large as about 600 μm. Consequently, the large distance increases the thermal resistance and limits the heat transfer from the functional materials filled into the pore space to the high-conductivity struts. Based on a previous report,[17] small pore size porous Ni templates can be obtained by sintering of small size Ni powder template. Here, Ni powder smaller than 20 μm is sintered within the temperature limit of the CVD furnace to form the Ni foam template without the use of a separate sintering process in a high-temperature furnace.

2.1.1 Growth of Hexagonal Boron Nitride Foam

High purity (99.9%) < 20 μm (-625 mesh) nickel powder (Atlantic Equipment Engineers) is used for the synthesis of the sintered Ni powder foam. Isopropyl alcohol (IPA) and 4g of nickel powder are loaded into a combustion crucible, which is placed in a tube furnace. The tube is purged with 45 sccm Ar and 5 sccm H_2 gas flow for 30 minutes to evaporate the IPA. At the same flowrates, the furnace temperature is ramped up slowly over five hours to 1080°C, which is held for 2 hrs to sinter the Ni powder. The scanning

electron microscopy result of well-merged, continuous sintered Ni powder foam is shown in **Figure 2.1**.

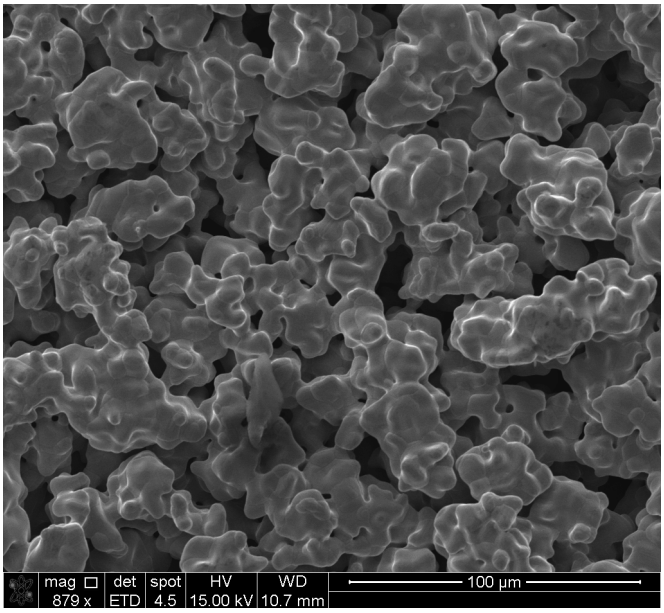

Figure 2.1: Scanning electron microscopy (SEM) images of a porous Ni foam obtained by sintering <20 µm (-625 mesh) powder

The APCVD system is shown in **Figure 2.2**(a), which contains a single-zone quartz tube furnace (Lindberg/Blue M Mini-mite), a band heater, a combustion crucible, a Ni template and gas supply. The combustion boat containing 700 mg of borane-ammonia complex powder (Sigma Aldrich) is placed at 10 cm away from the heating zone. Sintered Ni powder foam is cut into small piece and placed in the center of the quartz tube. The inner diameter (ID) and outer diameter (OD) of the quartz tube are 20 mm and 25.4 mm, respectively. The surface of the Ni foam is normal to the flow direction, as shown in **Figure 2.2**(b). The normal position allows the gas flow to penetrate though the pore of the sintered powder, which increases the h-BN growth rate compared to the parallel position shown in **Figure 2.2**(c) and used in prior experiments.[31-33]

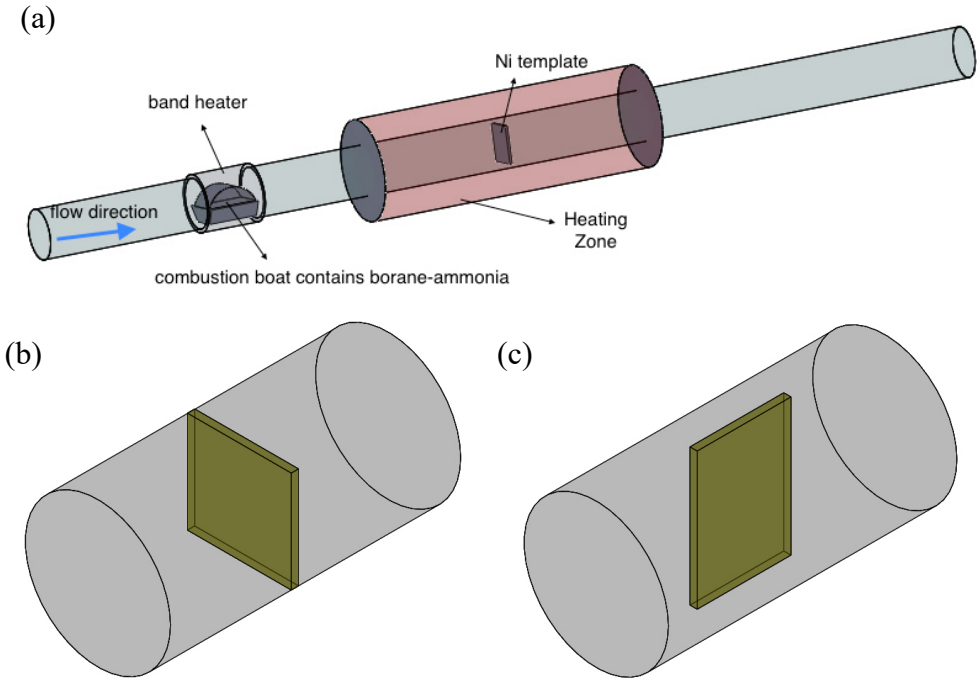

Figure 2.2: (a) Schematic diagram of a CVD system that contains a heating zone, a crucible loaded with borane-ammonia, a band heater, and a Ni template. The blue arrow indicates the flow direction. (b) Schematic illustration of the normal position of the Ni template. (c) Schematic illustration of the parallel position of the Ni template.

The sintered Ni powder foam template is first annealed under ultra-high purity H_2 gas at 90 sccm and atmospheric pressure for 2 hrs at 1080°C to reduce the surface oxide. Subsequently, the H_2 flow rate is increased to 360 sccm and the band heater is heated to 120°C to sublimate the borazane powder and grow h-BN on the sintered Ni powder template. After 1.5 hrs of growth, the quartz furnace is cooled down to room temperature in an Ar flow at 60 sccm. The grown h-BN on sintered-powder foam is shown in **Figure 2.3**.

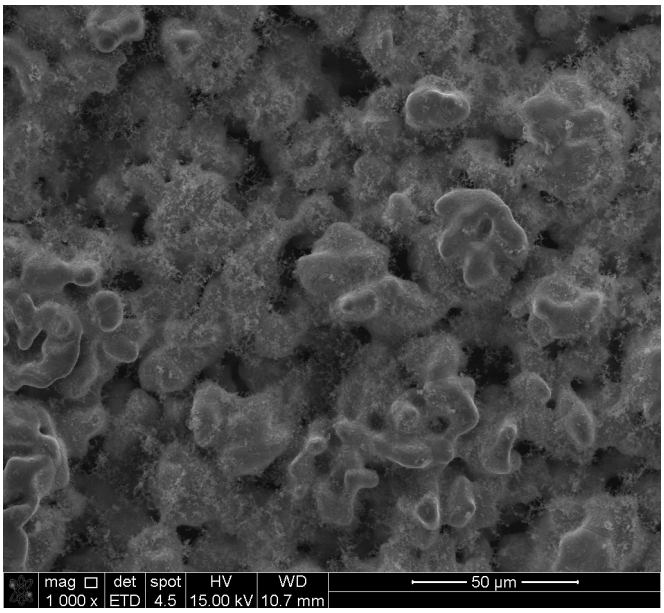

Figure 2.3: Scanning electron micrograph of h-BN grown on sintered Ni powder foam with < 20 µm powder size.

The as-grown sample is coated with droplets of 4 wt% PMMA to partially fill the open cellular structure. After the PMMA is cured at 100°C for 1 hr, the sample is immersed into 6M HCl on a hot plate at 100°C for 5 hrs to completely remove the nickel (**Figure 2.4**). Following etching and DI water rinsing, the PMMA-coated h-BN is dried overnight and then heated in the quartz tube at 400°C for 2 hrs under open air to burn off the PMMA. In comparison, removing the PMMA in acetone can destroy the structural integrity of the h-BN foam.

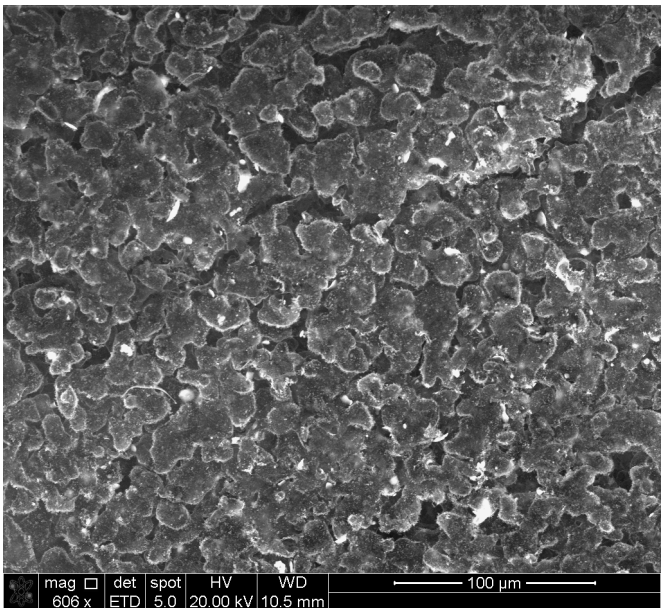

Figure 2.4: Scanning electron micrograph of h-BN foam upon the removal of the sintered Ni powder foam template

2.1.2 Synthesis of Hexagonal Boron Nitride –Polymer Composite

In addition to free-standing h-BN foam, h-BN–PMMA composite structure is prepared for thermal transport measurements. To minimize the air void volume fraction inside the h-BN-PMMA composite, 12 wt% PMMA solution is placed under vacuum for 10 mins before it is filled into the h-BN–Ni foam. The h-BN–Ni sample is then immersed in the PMMA solution and cured for 1 hr at 100°C. Due to the high-volume fraction of protective PMMA, the Ni in the composite is then etched with 6M HCL for 10 hrs. The h-BN–PMMA sample based on the sintered Ni powder template is shown in **Figure 2.5(a)**. As a comparison, the same fabrication process is carried out with a commercial Ni foam as the starting catalytic template to obtain baseline h-BN–PMMA composite. The baseline h-BN–PMMA composite is shown in **Figure 2.5(b)**. In addition, two h-BN samples grown on the sintered Ni powder template are annealed under 700°C in air for 24 and 48 hrs,

respectively. These annealed samples are used to prepare annealed h-BN–PMMA composites to investigate the effect of annealing on the thermal transport properties.

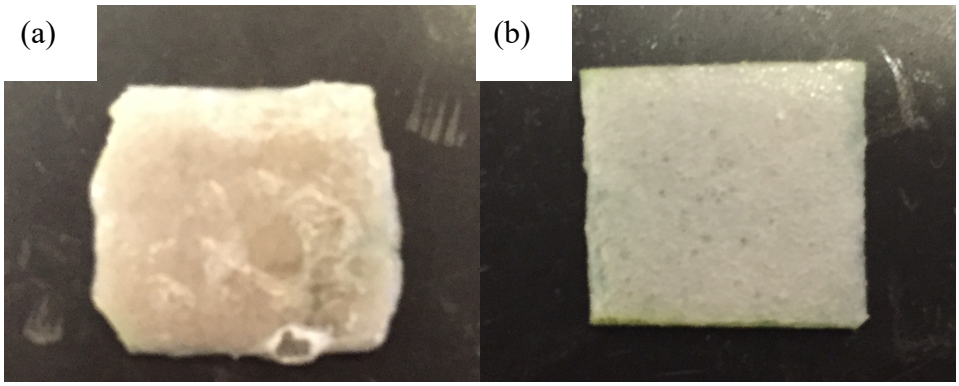

Figure 2.5: Optical graphs of h-BN-PMMA composites (a) based on sintered Ni foam template with < 20 μm powder and (b) based on commercial Ni foam template.

2.2 Characterization of High-Surface Area Hexagonal Boron Nitride Polymeric Composite

Because of the relatively small pore size of the sintered Ni powder foam, its specific surface is much higher than that of the commercial Ni foam. Consequently, the volume fraction ($\phi_{h\text{-}BN}$) of h-BN grown on the sintered template is 0.34 ± 0.059%, around 3 times of that of the reticulated Ni foam (0.12 ± 0.018%). The volume fraction is calculated from the h-BN mass, which is determined based on the mass increase upon the h-BN growth on the Ni template. Because the h-BN growth rate decreases as the solid precursor is used up, the h-BN strut wall thickness cannot be increased to the level found in the graphite foam grown with a gaseous carbon feedstock. The estimate h-BN strut wall thickness of sintered powder template is 70 ± 10nm based on the spherical powder approximation and specific surface area. Although the specific surface area of the sintered Ni template is increased considerably, the h-BN volume fraction is still well below 1% and much smaller than the graphite volume fraction in graphite foam-polymer composite.

Meanwhile, the reduced pore size increases the viscous force for the PMMA flow, increasing the difficulty of filling PMMA into the pores. In particular, the sintered powder foam has a porosity of 72.5%, lower than that of reticulated Ni foam (97.1%). Therefore, the Ni volume fraction increases from 2.9% to 27.5% in the Ni template. Upon h-BN growth, Ni etching, and PMMA filling, the original space occupied by Ni was either compressed by the PMMA or partially filled by the PMMA. However, it is more difficult for the PMMA to fill in this space than in the larger pore space originally occupied by air. Consequently, the volume fraction of PMMA (ϕ_{PMMA}) decreases from 44% for the h-BN–PMMA composite sample prepared from the reticular Ni foam template to around 34% for the sample prepared from the sintered Ni template. The remaining volume fraction is occupied by air pockets trapped in the composite. The effective density ($\rho_{eff,c}$) of the h-BN–PMMA composite is dominated by the PMMA fraction and varies from 0.3g/cc-0.34g/cc, as shown in **Table 2.1**.

Table 2.1: Room-temperature measurement results for PMMA, baseline h-BN foam samples grown on a reticulated Ni foam template, high surface area h-BN foam samples grown on sintered-powder templates.

Sample	$\rho_{eff,c}$ (g/cc)	$\phi_{h\text{-}BN}$ *(vol. %)*	$\alpha_{eff,c}$ (mm^2/s)	$\kappa_{eff,c}$ ($Wm^{-1}K^{-1}$)	$\kappa_{eff,h-BN}$ ($Wm^{-1}K^{-1}$)	κ_{solid} ($Wm^{-1}K^{-1}$)
PMMA	0.99±0.02	-	0.15±0.04	0.21±0.06	-	0.21±0.06
baseline h-BN-PMMA composite	0.30±0.002	0.12±0.02	0.70±0.01	0.31±0.02	0.23±0.03	510±170
High surface area h-BN-PMMA composite	0.32±0.003	0.34±0.06	1.12±0.01	0.51±0.04	0.44±0.04	380±80

Raman Spectroscopy is used to characterize the APCVD grown h-BN. Multiple locations on h-BN grown on both the Ni foam and sintered Ni powder templates are measured and similar results are obtained. **Figure 2.6** shows the typical Raman spectra of the h-BN before and after the removal of the Ni templates and after 48 hrs of post-annealing. The clear peaks at around 1370 cm^{-1} indicate crystalline h-BN grown by the APCVD method.[34]

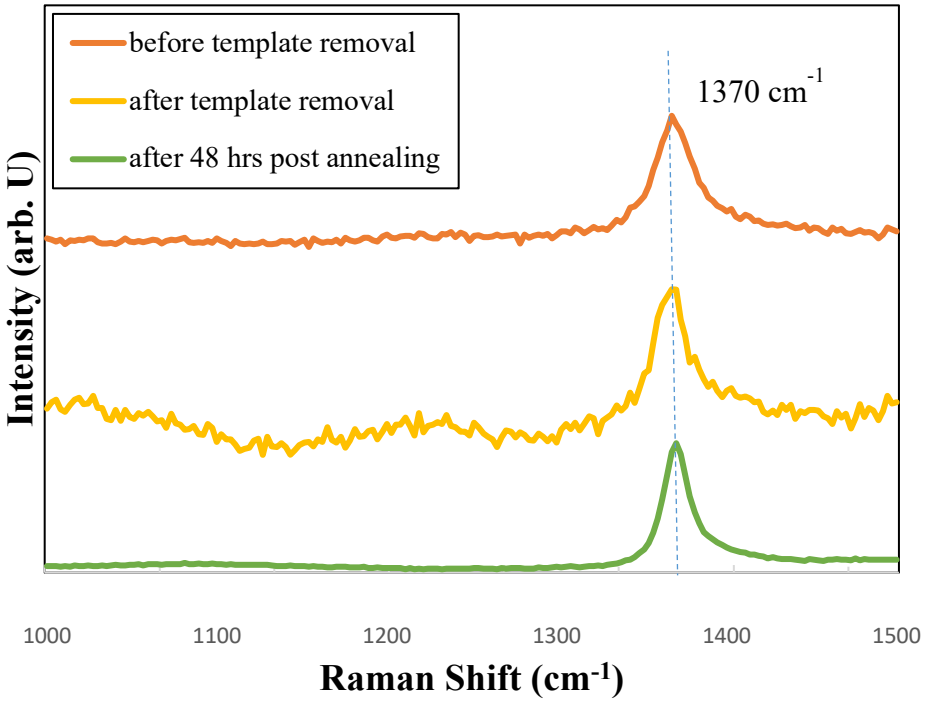

Figure 2.6: Raman spectrum of h-BN before (red line) and after (orange line) the removal of Nickel template and PMMA, and after 48 hrs post annealing (green line).

Thermal properties of h-BN-PMMA composite are measured via Laser Flash Analysis (Netzsch LFA 457 Microflash) and Differential Scanning Calorimetry (Netazch DSC 404 F1 Pegasus). PMMA is one of the polymers used in electronics displays, lighting, and automotive applications. These polymers typically have very low thermal conductivity.

Although the h-BN volume fraction is less than 1%, the interconnected h-BN open cell structure increases the effective thermal conductivity of the composite, which is obtained as

$$\kappa_{eff,c} = \alpha_{eff,c}\rho_{eff,c}C_{eff,c} \quad (2.1)$$

where the $\rho_{eff,c}$ is the measured density of the h-BN-PMMA composite, $\alpha_{eff,c}$ is the composite effective thermal diffusivity determined via LFA and $C_{e,c}$ is the effective heat capacity calculated via the rule of mixture

$$C_{eff,c} = \frac{m_{PMMA}}{m_c} * C_{PMMA} + \frac{m_{h-BN}}{m_c} * C_{h-BN} + \frac{m_{air}}{m_c} * C_{air} \quad (2.2)$$

Where C_{PMMA}, C_{h-BN} and C_{air} are literature results of material's heat capacity, m_c, m_{h-BN}, m_{PMMA}, and m_{air} are the mass of the h-BN-PMMA composite, h-BN, PMMA, and air void in the composites, respectively. $C_{eff,c}$ is further verified with DSC where the calculated result based on the rule of mixture is within 10% uncertainty of the measured result. The C_{PMMA}, C_{h-BN} and C_{air} used in the calculation are 1.42 J/g K, 0.72 J/g K and 1.0 J/g K, respectively. The contribution of h-BN to the composite effective thermal conductivity is calculated as

$$\kappa_{eff,h-BN} = \kappa_{eff,c} - \phi_{PMMA}\kappa_{PMMA} \quad (2.3)$$

The $\kappa_{eff,c}$ of the h-BN-PMMA composites based on the sintered Ni powder template and commercial Ni foam are plotted in **Figure 2.7**, in comparison with the κ results of pure PMMA measured in this work and reported in the literature.[35,36] At room temperature, the measured pure PMMA sample yields a solid thermal conductivity of 0.21 ± 0.06 $Wm^{-1}K^{-1}$, which matches the reference result.[35,36] By adding the h-BN as a matrix, the h-BN–PMMA composite based on the commercial Ni foam obtains a $\kappa_{eff,c}$ value of 0.31 ± 0.02 $Wm^{-1}K^{-1}$, around 1.5 times of pure PMMA. Despite the presence of the air void, the effective thermal conductivity is enhanced due to the contribution from the continuous h-BN foam structure. In addition, the high surface area h-BN–PMMA composite achieves

an effective thermal conductivity value of 0.51 ± 0.04 $Wm^{-1}K^{-1}$, which is 2.4 times that of the pure PMMA and 1.7 times that of the baseline h-BN–PMMA composite. Although the air void fraction is increased in this small pore size structure, the effective thermal conductivity is increased further because of a 3-fold increase of the h-BN volume fraction compared to the baseline foam. The h-BN contribution to the effective thermal conductivity increases from 0.23 ± 0.03 $Wm^{-1}K^{-1}$ for the baseline composite to 0.44 ± 0.04 $Wm^{-1}K^{-1}$ for the high-surface area h-BN–PMMA composite. In addition, the solid thermal conductivity of bulk h-BN increases with decreasing temperature[37] due to reduced phonon-phonon scattering, whereas κ_{PMMA} shows an opposite trend owing to its amorphous structure.[35,36] Thus, the thermal enhancement with the h-BN foam is expected to be more pronounced at a lower temperature.

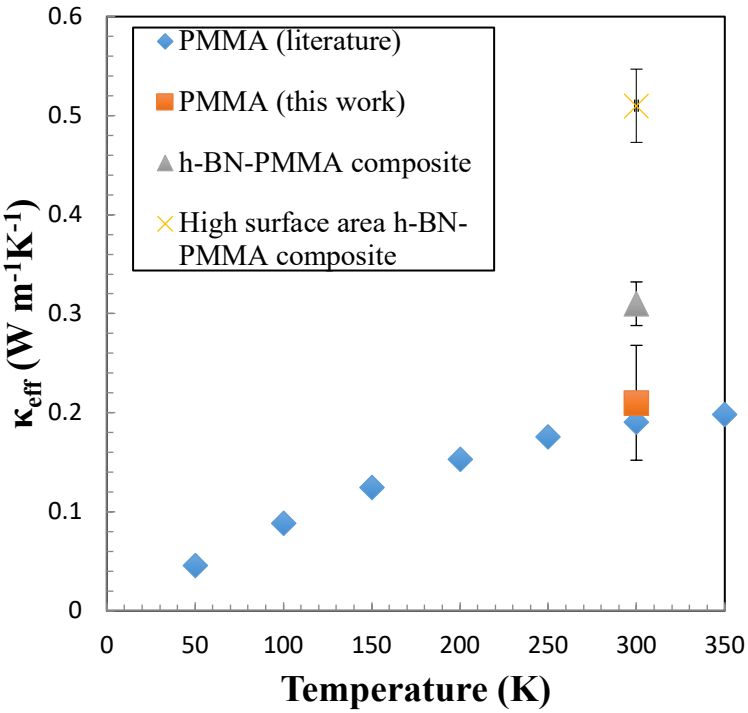

Figure 2.7: Effective thermal conductivity of the h-BN-PMMA composites prepared with the commercial Ni foam template (baseline) and the high-surface area sintered-powder template, respectively, in comparison with the measured and literature values of PMMA.[35,36]

The solid thermal conductivity of h-BN can be determined via Lemlich foam model.[38] With the assumption of 3D isotropic heat conduction and parallel thermal contribution of PMMA and h-BN, the h-BN solid thermal conductivity can be evaluated as

$$\kappa_{solid,h-BN} = 3\frac{k_{eff,c}-\phi_{PMMA}\kappa_{PMMA}}{\phi_{h-BN}} \quad (2.4)$$

where Φ_{PMMA} and $\Phi_{h\text{-}BN}$ are the volume fractions of PMMA and h-BN of the composite, respectively and κ_{PMMA} is determined via same process as the h-BN-polymer composite. While the sintered Ni powder template has a relatively low uniformity compared to the cellular structure of reticulated Ni foam, the thickness of the grown h-BN is much smaller

than the pore size of the sintered foam. Therefore, the Lemlich foam model is used here to evaluate the solid thermal conductivity of the high-surface area h-BN foam. As shown in **Figure 2.8** and **Table 2.1**, the solid thermal conductivity of high-surface area h-BN foam is 380 ± 80 $Wm^{-1}K^{-1}$, which is close to the literature basal-plane values of h-BN crystals with natural isotopic impurities. [37] Despite the approximation in the Lemlich model, the obtained solid thermal conductivity indicates the good crystalline quality of the grown h-BN.

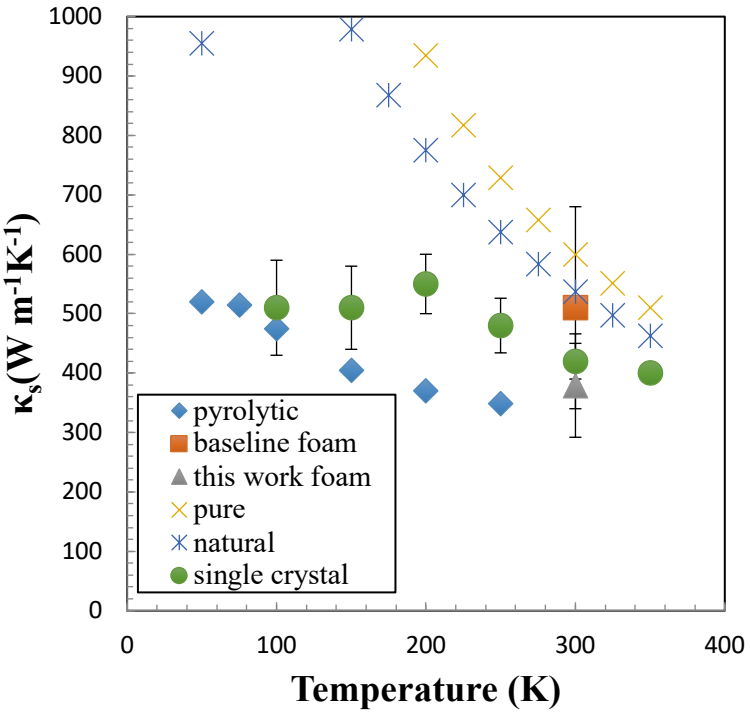

Figure 2.8: Basal-plane thermal conductivity of the h-BN struts grown on the commercial Ni foam template and the sintered-powder template, respectively, in comparison with literature measurement results of a h-BN single crystal sample[37] and a pyrolytic compression annealed h-BN sample[18] and theoretical results for h-BN bulk crystals with naturally occurring isotopic impurities.[37]

The specific thermal conductivity is an important measure for conductive foams in applications where weight is an important factor.[39] This property is calculated as the solid

thermal conductivity divided by the bulk density of the foam strut, with a value of 0.045W m^2 kg^{-1} K^{-1} for copper foam.[39] The calculated specific thermal conductivity of h-BN foam based on the reticulated Ni foam is 0.26 W m^2 kg^{-1} K^{-1}, which is about 6 times greater than the value for copper foam and close to the specific thermal conductivity of ultrathin-graphite foam, 0.32 W m^2 kg^{-1} K^{-1}.[17]

The results for the annealed h-BN-PMMA composite samples are shown in **Table 2.2**. The volume fractions of h-BN and PMMA are comparable for these samples, resulting in similar effective densities in the range between 0.3g/cc and 0.34g/cc. With different post annealing times, the enhancement of the effective thermal conductivity of the composite varies. The annealing increases the mean value of the measured solid thermal conductivity for only the h-BN grown on the sintered Ni powder template but not on the reticular Ni foam template. Nevertheless, the increase is still comparable to the uncertainty of the value.

Table 2.2: Measurement results of three samples with different post annealing times

Sample	Post anneal time	$\phi_{h\text{-}BN}$ *(vol. %)*	ϕ_{PMMA} *(vol. %)*	$\kappa_{eff,c}$ ($Wm^{-1}K^{-1}$)	κ_s ($Wm^{-1}K^{-1}$)
Sample 1	-	0.34±0.06	34.9±0.2	0.51±0.04	380±80
Sample 2	24 hrs	0.29±0.06	33.0±0.2	0.52±0.04	470±110
Sample 3	48 hrs	0.30±0.06	34.0±0.2	0.60±0.05	490±120

Figure 2.9 compares the effective composite thermal conductivity of the high surface area h-BN–PMMA foam with the values of the baseline foam-like h-BN-PMMA composite,[33] ultra-thin graphite foam (UGF) loaded with wax,[6] few-layer BN nanosheet-epoxy composite,[40] and h-BN platelets-linear low-density polyethylene (LLDPE) matrix.[41] Despite a much lower volume fraction of the high-thermal conductivity filler, the h-BN foam composite obtains an effective thermal conductivity comparable to the other samples.

The effective thermal conductivity can potentially be increased further by increasing the surface area of the sintered Ni powder template via an optimization of the powder size and the sintering temperature.

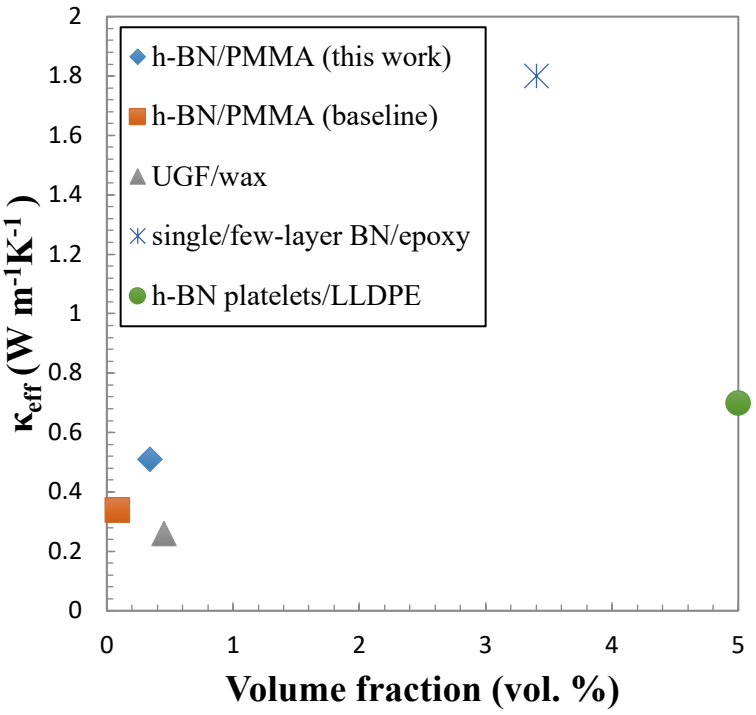

Figure 2.9: Comparison of the effective thermal conductivity of the high surface area h-BN foam sample and other porous foam composites, including baseline h-BN-PMMA foam,[33] ultra-thin graphite foam (UGF)-wax composite,[6] few-layer BN-epoxy composite,[40] and h-BN platelets-LLDPE composite.[41]

Chapter 3 Conclusion

This thesis is focused on the synthesis and characterization of high surface area h-BN foam for thermal management applications. With low-cost nickel powders, a small-pore-size Ni template can be sintered for CVD-growth of high-surface area h-BN foam structure. An APCVD method is used grow h-BN foams on both sintered Ni powder template and reticular Ni foam template. As a common polymer, PMMA is used to infiltrate both h-BN foams to make composite structures. The continuous, interconnected foam-like structure helps to eliminate the internal contact resistance while enhancing the heat transfer between the loaded functional material and h-BN strut. With an order of magnitude smaller pore size and an order of magnitude higher specific surface area than that of reticulated Ni foam, the high-surface area h-BN-PMMA composite increases the volume fraction of h-BN from $0.12 \pm 0.02\%$ to $0.34 \pm 0.06\%$ and yields an effective thermal conductivity increase from 0.31 ± 0.02 $Wm^{-1}K^{-1}$ to 0.51 ± 0.04 $Wm^{-1}K^{-1}$ at room temperature. The solid thermal conductivity obtained from the high-surface area h-BN composite is 380 ± 80 $Wm^{-1}K^{-1}$, which is close to the literature basal-plane value of h-BN crystal with natural isotopic impurities. In comparison with other porous network fillers, the high-surface area h-BN foam achieves a reasonably high effective thermal conductivity at a volume fraction well below 1%. It appears that the solid thermal conductivity of the h-BN grown on the sintered Ni powder template can be increased with high-temperature annealing to reduce defects. Future work to further improve on these concepts includes optimizing the powder size and sintering temperature to further increase the specific surface area and porosity, eliminating air voids to increase the effective composite density, adjusting growth and post-process parameters, and exploring different etchant methods.

References

[1] Moore, B. G. E. (1965). Cramming more components onto integrated circuits. *Electronics*, *38*(8).

[2] Pop, E. (2008). The role of electrical and thermal contact resistance for Joule breakdown of single-wall carbon nanotubes. *Nanotechnology*, *19*(295202).

[3] Rotkin, S. V, Perebeinos, V., Petrov, A. G., & Avouris, P. (2009). An Essential Mechanism of Heat Dissipation in Carbon Nanotube Electronics. *Nano Letters*, *9*(5), 1850–1855.

[4] Moore, A. L., & Shi, L. (2014). Emerging challenges and materials for thermal management of electronics. *Materials Today*, *17*(4), 163–174.

[5] Lafdi, K., Mesalhy, O., & Shaikh, S. (2007). The effect of surface energy on the heat transfer enhancement of paraffin wax / carbon foam composites. *Carbon*, *45*, 2188–2194.

[6] Pettes, M. T., Ji, H., Ruoff, R. S., & Shi, L. (2012). Thermal transport in three-dimensional foam architectures of few-layer graphene and ultrathin graphite. *Nano Letters*, *12*(6), 2959–2964.

[7] Tao, X., Chen, X., Xia, Y., Huang, H., Gan, Y., Wu, R., Chen Wu, zhang, W. (2013). Highly mesoporous carbon foams synthesized by a facile, cost-effective and template-free Pechini method for advanced lithium–sulfur batteries. *Journal of Materials Chemistry A*, *1*(10), 3295-3301.

[8] Klett, J. W., Millan, a D. M. C., Gallego, N. C., Walls, C. a, Division, C., & Ridge, O. (2004). The role of structure on the thermal properties of graphitic foams. *Journal of Materials Science*, *9*(11), 3659–3676.

[9] Zhao, C. Y., & Wu, Z. G. (2011). Heat transfer enhancement of high temperature thermal energy storage using metal foams and expanded graphite. *Solar Energy Materials and Solar Cells*, *95*(2), 636–643.

[10] Focke, W. W., Badenhorst, H., Ramjee, S., Kruger, H. J., Van Schalkwyk, R., & Rand, B. (2014). Graphite foam from pitch and expandable graphite. *Carbon*, *73*, 41–50.

[11] He, Y., Liu, Y., Wu, T., Ma, J., Wang, X., Gong, Q., Kong, W., Xing, F., Liu, Y., & Gao, J. (2013). An environmentally friendly method for the fabrication of reduced graphene oxide foam with a super oil absorption capacity. *Journal of Hazardous Materials*, *260*, 796–805.

[12] Karthik, M., Faik, A., & D'Aguanno, B. (2017). Graphite foam as interpenetrating matrices for phase change paraffin wax: A candidate composite for low temperature thermal energy storage. *Solar Energy Materials and Solar Cells*, *172*(April), 324–334.

[13] Inagaki, M., Qiu, J., & Guo, Q. (2015). Carbon foam: Preparation and application. *Carbon*, *87*(C), 128–152.

[14] Ji, H., Zhang, L., Pettes, M. T., Li, H., Chen, S., Shi, L., Piner, R., &Ruoff, R. S. (2012). Ultrathin graphite foam: A three-dimensional conductive network for battery electrodes. *Nano Letters*, *12*(5), 2446–2451.

[15] Kholmanov, I., Kim, J., Ou, E., Ruoff, R. S., & Shi, L. (2015). Continuous Carbon Nanotube-Ultrathin Graphite Hybrid Foams for Increased Thermal Conductivity and Suppressed Subcooling in Composite Phase Change Materials. *ACS Nano*, *9*(12), 11699–11707.

[16] Yan, Z., Ma, L., Zhu, Y., Lahiri, I., Hahm, M. G., Liu, Z., … Tour, J. M. (2013). Three-Dimensional Metal À Graphene À Nanotube Multifunctional Hybrid Materials, (1), 58–64. https://doi.org/10.1021/nn3015882

[17] Fleming, E., Kholmanov, I., & Shi, L. (2018). Enhanced specific surface area and thermal conductivity in ultrathin graphite foams grown by chemical vapor deposition on sintered nickel powder templates. *Carbon*, *136*, 380–386.

[18] Sichel, E. K., Miller, R. E., Abrahams, M. S., & Buiocchi, C. J. (1976). Heat capacity and thermal conductivity of hexagonal pyrolytic boron nitride. *Physical Review B*, *13*(10), 4607–4611.

[19] Rubio, A., Corkill, J. L., & Cohen, M. L. (1994). Theory of graphitic boron nitride nanotubes. *Physical Review B*, *49*(7), 5081–5084.

[20] Alem, N., Erni, R., Kisielowski, C., Rossell, M. D., Gannett, W., & Zettl, A. (2009). Atomically thin hexagonal boron nitride probed by ultrahigh-resolution transmission electron microscopy. *Physical Review B*, *80*(15), 1–7.

[21] Li, X., Yan, Y., Dong, L., Guo, J., Aiyiti, A., Xu, X., & Li, B. (2017). Thermal conduction across a boron nitride and SiO 2 interface. *Journal of Physics D: Applied Physics*, *50*(10).

[22] Zhang, K., Feng, Y., Wang, F., Yang, Z., & Wang, J. (2017). Two dimensional hexagonal boron nitride (2D-hBN): Synthesis, properties and applications. *Journal of Materials Chemistry C*, *5*(46), 11992–12022.

[23] Kim, K. K., Hsu, A., Jia, X., Kim, S. M., Shi, Y., Dresselhaus, M., & Al, K. I. M. E. T. (2012). Synthesis and Characterization of Hexagonal Boron Nitride Film as a Dielectric Layer for Graphene Devices. *ACS Nano*, *6*(10), 8583–8590.

[24] Qi, Z. J., Hong, S. J., Rodríguez-Manzo, J. A., Kybert, N. J., Gudibande, R., Drndic, M., Park, Y.W., Johnson, A. T. C. (2015). Electronic transport in heterostructures of chemical vapor deposited graphene and hexagonal boron nitride. *Small*, *11*(12), 1402–1408.

[25] Loeblein, M., Tay, R. Y., Tsang, S. H., Ng, W. B., & Teo, E. H. T. (2014). Configurable three-dimensional boron nitride-carbon architecture and its tunable electronic behavior with stable thermal performances. *Small*, *10*(15), 2992–2999.

[26] Lee, K. H., Shin, H., Lee, J., Lee, I., Kim, G., Choi, J., & Kim, S. (2012). Large-Scale Synthesis of High-Quality Hexagonal Boron Nitride Nanosheets for Large-Area Graphene Electronics. *Nano Letters*, *12*, 714–718.

[27] Lee, C., Kybert, N. J., Lerner, M. B., Han, G. H., & Rodrı, J. A. (2013). Continuous Growth of Hexagonal Graphene and Boron Nitride In-Plane Heterostructures by Atmospheric Pressure Chemical Vapor Deposition. *ACS Nano*, *7*(11), 10129–10138.

[28] Tay, R. Y., Griep, M. H., Mallick, G., Tsang, S. H., Singh, R. S., Tumlin, T., … Karna, S. P. (2014). Growth of Large Single-Crystalline Two-Dimensional Boron Nitride Hexagons on Electropolished Copper. *Nano Letters*, *14*, 839–846.

[29] Tay, Roland Yingjie, Xingli Wang, Siu Hon Tsang, Guan Chee Loh, Ram Sevak Singh, Hong Li, Govind Mallick, and Edwin Hang Tong Teo. (2014). A Systematic Study of the Atmospheric Pressure Growth of Large-Area Hexagonal Crystalline Boron Nitride Film. *Journal of Materials Chemistry C* 2 (9): 1650–1657.

[30] Koepke, J. C., Wood, J. D., Chen, Y., Schmucker, S. W., Liu, X., Chang, N. N., Nienhaus, L., Do, J. W., Carrion, E. A., Hewaparakrama, J., Rangarajan, A., Datye, I., Mehta, R., Haasch, R. T., Gruebele, M., Girolami, G. S., Pop, E., &Lyding, J. W. (2016). Role of pressure in the growth of hexagonal boron nitride thin films from ammonia-borane. *Chemistry of Materials*, *28*(12), 4169–4179.

[31] Yin, J., Li, X., Zhou, J., & Guo, W. (2013). Ultralight Three-Dimensional Boron Nitride Foam with Ultralow Permittivity and Superelasticity. *Nano Letters*, *13*, 3232–3236.

[32] Ashton, T. S., & Moore, A. L. (2015). Three-dimensional foam-like hexagonal boron nitride nanomaterials via atmospheric pressure chemical vapor deposition. *Journal of Materials Science*, *50*(18), 6220–6226.

[33] Ashton, T. S., & Moore, A. L. (2017). Foam-like hierarchical hexagonal boron nitride as a non-traditional thermal conductivity enhancer for polymer-based composite materials. *International Journal of Heat and Mass Transfer*, *115*, 273–281.

[34] Gorbachev, R. V., Riaz, I., Nair, R. R., Jalil, R., Britnell, L., Belle, B. D., Hill, W. W., Novoselov, K.S., Watanabe, K., Taniguchi, T., & Blake, P. (2011). Hunting for monolayer boron nitride: Optical and Raman signatures. *Small*, *7*(4), 465–468.

[35] Cahill, D. G., & Pohl, R. O. (1987). Thermal conductivity of amorphous solids above the plateau, *Physical Review B*, *35*(8), 4067–4073.

[36] Assael, M. J., Botsios, S., Gialou, K., & Metaxa, I. N. (2005). Thermal Conductivity of Polymethyl Methacrylate (PMMA) and Borosilicate Crown Glass BK7. *International Journal of Thermophysics*, *26*(5), 1595–1605.

[37] Jiang, P., Qian, X., Yang, R., & Lindsay, L. (2018). Anisotropic thermal transport in bulk hexagonal boron nitride. *Physical Review Materials 2*, *064005*, 1–8.

[38] Lemlich, R. (1978). A theory for the limiting conductivity of polyhedral foam at low density. *Journal of Colloid And Interface Science*, *64*(1), 107–110.

[39] Klett, J., Hardy, R., Romine, E., Walls, C., & Burchell, T. (2000). High-thermal-conductivity, mesophase-pitch-derived carbon foams: effect of precursor on structure and properties. *Carbon*, *38*, 953–973.

[40] Lin, Z., Yao, Y., Mcnamara, A., Moon, K., & Wong, C. P. (2012). Single / few-layer Boron Nitride-based Nanocomposites for High Thermal Conductivity Underfills. *2012 IEEE 62nd Electronic Components and Technology Conference*, 1437–1441.

[41] Chan, E., Leung, S. N., Khan, M. O., Naguib, H. E., Dawson, F., & Adinkrah, V. (2012). Novel thermally conductive thermoplastic/ceramic composite foams. *Macromolecular Materials and Engineering*, *297*(10), 1014–1020.